Seismic Performance of Steel-Braced Frames with an All-Steel Buckling Restrained Brace

Mehdi Ebadi Jamkhaneh, S.M.ASCE[1]; Amir Homaioon Ebrahimi, Ph.D.[2]; and Maedeh Shokri Amiri, M.Sc.[3]

Abstract: In terms of weight and curing of mortar in the brace core, an all-steel buckling-restrained brace is considered an improved type of common buckling-restrained brace. In this study, a new type of all-steel buckling-restrained brace was introduced; it was made up of three parallel plates that were connected through a Z-shaped profile. Cyclic analysis was conducted through a software program for finite-element analysis. First, the numerical model was validated through an experimental sample, and the finite-element numerical model was introduced after achieving a desirable match with the behavior of the model. The variable parameters of this analysis were the overlap length of the plates and the section depth of the brace. Determination of the nonlinear modeling parameters of the brace was followed by comparison of two modes of the frame with typical convergent X-shaped braces and buckling-restrained braces for 5-, 10-, and 15-story structures through pushover and nonlinear time-history analyses. The obtained results suggest that the new buckling-restrained brace maintained the structural-life safety performance level. **DOI: 10.1061/(ASCE)SC.1943-5576.0000381.** *© 2018 American Society of Civil Engineers.*

Author keywords: New all-steel buckling-restrained brace; Finite-element analysis; Performance level; Behavior coefficient; Nonlinear time-history analysis.

Introduction

Steel braces are commonly used for resisting wind and seismic loads in structural systems. Because of periodic loading and compressive buckling, these elements have reduced resistance and stiffness when used in seismic areas. In the 1970s, buckling-restrained braces (BRBs) were introduced to prevent the buckling of braces under alternating seismic loads. Wakabayashi et al. (1973) introduced a bracing system made up of a steel core surrounded by two prefabricated concrete wall panels. Kimura et al. (1976) introduced another type of BRB by placing a core in a steel tube filled with cement mortar. Mochizuki et al. (1979) suggested a set of tests on braces with a layer of shock absorber materials that prevent bonding between the steel core and the concrete. The absorbent material allows the steel core to move transversely under compressive loads. These sorts of BRBs are called *unbonded braces*. In general, a buckling-restrained or unbonded brace consists of three parts: a steel core, buckling-restrained sheath, and slippery material between the core and the sheath. Wada et al. (1989) suggested that a BRB could be designed as a damper that dissipates the seismic energy input to the structure. Black et al. (2002) and Merritt et al. (2003) conducted low-cycle fatigue tests to evaluate the behavior of BRBs. Despite the advantages of them, several weaknesses of BRBs need to be addressed. The disadvantages include complexity of boundary conditions of contact between materials and elements,

time-consuming production processes, and difficulty in determining the destruction after an earthquake.

As a practical solution, all-steel BRBs that did not require slipping material or mortar were suggested for dealing with the disadvantages of BRBs (Fahnestock et al. 2007). The braces were made up of a steel core and a sheath; the sheath was solely controlled through a created gap between the core and sheath along the buckling direction. Tsai et al. (2004) and Tsai and Hsiao (2008) introduced a new type of all-steel multicurve BRB. Zhao et al. (2011) conducted a study on multicurved buckling restrained brace (MC-BRB) and concluded that these braces have more stable mechanical characteristics than common BRBs, and they do not require slippery materials. In 2013, the behavior of large-scale all-steel MC-BRBs, composed of two steel cores for bearing a 1,400-kN axial load, was studied (Tsai et al. 2012). The results suggested that the braces with two steel plates in the cores showed stable mechanical behavior under cyclic loading and desirable inelastic plasticity capacity. Hoveidae and Rafezy (2012) studied the general buckling behavior of all-steel BRBs. They conducted analytical studies on BRBs with different gaps between the core and the buckling-restrained element. The results suggested that bending stiffness of all-steel BRBs could significantly affect their general buckling behavior. Hosseinzadeh and Mohebi (2016) studied the behavior of an all-steel BRB by considering different gaps between the core and steel sheath. In their study, a comparison of the behavior of the brace with that of a typical convergent X-brace indicated that the use of all-steel BRBs maintained the seismically loaded structure within a life-safety area. Zhu et al. (2017) suggested a modified shape of a BRB for attaining higher resistance against out-of-plane buckling. The method could represent desirable buckling resistance against high and severe seismic loads.

In the present study, a new shape of a BRB, with certain differences from previous prototypes, was introduced. The system was made up of three parallel steel plates with sufficient stiffness and strength. The plates distributed the force between plates, which were placed in the system in relation to the weak axis. As a result, absorption of energy was done in a directed manner because plastic joints were developed for the top and bottom of each plate and were

[1]Ph.D. Candidate, Faculty of Civil Engineering, Semnan Univ., Semnan, Iran (corresponding author). E-mail: mehdi.ebadi1985@hotmail.com

[2]Researcher, School of Engineering, Univ. of Birmingham, Birmingham, U.K. E-mail: homaioon.ebrahimi@yahoo.com

[3]Graduate Student, Urban Planning, Islamic Azad Univ., Science and Research Branch, Tehran, Iran. E-mail: oceanship9@gmail.com

© ASCE   04018016-1   Pract. Period. Struct. Des. Constr.

Pract. Period. Struct. Des. Constr., 2018, 23(3): 04018016

connected to the parallel plates. The height and thickness of the plates inside the system were variable, and resistance, stiffness, and ductility of the system could be altered by changing the number, thickness, and height of the plates used. The behavior of this system was initially studied under cyclic loading. Then, behavioral comparisons of 5-, 10-, and 15-story steel structures with typical convergent X-braces and the suggested brace were made through nonlinear static and dynamic analyses such that the drift ratio and lateral load capacity of the structure, as well as the ductility and distribution of the plastic joints, could be determined.

Finite-Element Modeling of the Proposed BRBs

Numerical cyclic analysis was conducted on nine specimens using the *Abaqus v6.14.2* program to study the behavior of the suggested BRBs. Three-dimensional (3D) models were applied to gain a correct and better understanding of the behavior of this type of bracing. These models included three plates of equal size, and the overlapping length of the plates and the distances between the plates were considered variable. The details of the brace sections and the sizes of the nine numerical models of the suggested bracing are listed in Table 1. Section names were based on the term B_xG_y, where B, x, and y indicate the first word of the bracing, the overlapping plate length to the total bracing length ratio, and

the distance of two plates from the plate widths of each other, respectively. The total length of the bracing of all specimens was equal to 2 m. Because of the difference in the overlapping lengths ratio, the plate lengths also varied.

Static cycle analysis was carried out using the standard *Abaqus v6.14.2* program. All the bracing model members were meshed using C3D8R reduced-integral first-order elements. Considering the program specifications, the maximum and minimum increments were considered 0.2 and 0.0001, respectively. Whereas Z-shaped profiles were subject to severe shear forces between the plates, a hexa-structured-elements mesh was considered to be approximately equal to 10 mm, and other parts, which were expected to remain in the linear region, were meshed with bigger sizes. Whereas the contact between the plates and Z-shaped members were of the welded type, tie constraints were used to connect the nodes on the surfaces of the plates with the Z-shaped profile. All the suggested bracing steel members were made from ST37 steel (yield strength of 370 MPa, Poisson's coefficient of 0.3, Young's modulus of 200 GPa).

A nonlinear isotropic-kinematic combined hardening rule was used to reproduce the plastic behavior of the materials. The selection and calibration of the steel material properties and the hardening parameters were based on the results of a coupon test conducted by Tremblay et al. (2006). Accordingly, it was decided that the finite-element (FE) results of this study were to be verified based on the Tremblay et al. (2006) study. The initial kinematic hardening

Table 1. Properties of BRB Specimens

Specimen	Model name	Plate dimensions $[D \times l' \times t_P(\text{mm})]$	Z-shape dimensions $[b \times h \times t_s(\text{mm})]$	B (mm)	K_0 (kN/mm)
1	$B_{0.25}G_{0.5}$	$200 \times 1{,}250 \times 10$	$50 \times 35 \times 5$	100	142.00
2	$B_{0.25}G_{1.0}$	$200 \times 1{,}250 \times 10$	$50 \times 85 \times 5$	100	36.75
3	$B_{0.25}G_{1.5}$	$200 \times 1{,}250 \times 10$	$50 \times 135 \times 5$	100	11.77
4	$B_{0.5}G_{0.5}$	$200 \times 1{,}500 \times 10$	$50 \times 35 \times 5$	200	211.71
5	$B_{0.5}G_{1.0}$	$200 \times 1{,}500 \times 10$	$50 \times 85 \times 5$	200	50.64
6	$B_{0.5}G_{1.5}$	$200 \times 1{,}500 \times 10$	$50 \times 135 \times 5$	200	25.30
7	$B_{0.75}G_{0.5}$	$200 \times 1{,}750 \times 10$	$50 \times 35 \times 5$	300	249.96
8	$B_{0.75}G_{1.0}$	$200 \times 1{,}750 \times 10$	$50 \times 85 \times 5$	300	103.22
9	$B_{0.75}G_{1.5}$	$200 \times 1{,}750 \times 10$	$50 \times 135 \times 5$	300	64.26

Note: D = width of brace; l' = length of each plate; t_p = thickness of plate; B = overall depth of brace; K_0 = initial elastic stiffness.
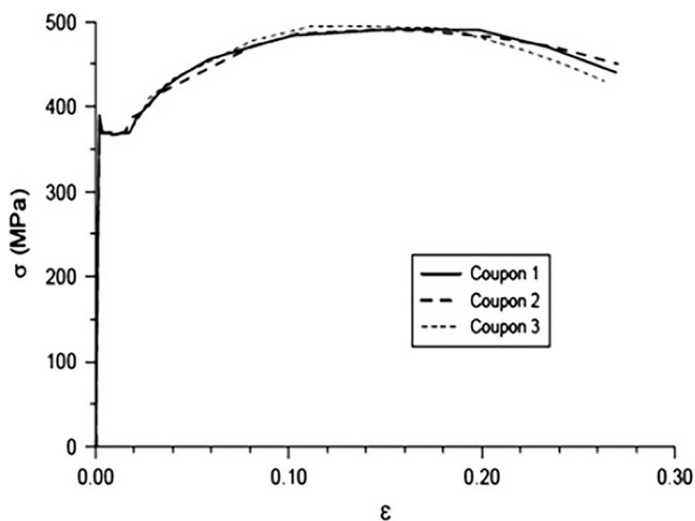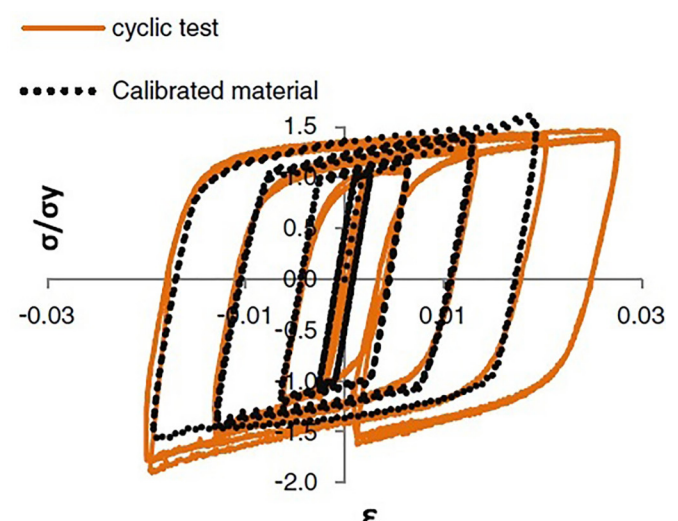
Fig. 1. (a) Monotonic experimental stress-strain curve; (b) cyclic experimental stress-strain curve and calibrated hysteretic response of the steel material

© ASCE 04018016-2 Pract. Period. Struct. Des. Constr.

Pract. Period. Struct. Des. Constr., 2018, 23(3): 04018016

modulus, C, and the rate factor, γ, were set to 8 GPa and 75, respectively. The material isotropic hardening parameters of the exponential law, Q_∞ and b, were chosen as 110 MPa and 4, respectively, according to Korzekwa and Tremblay (2009).

Fig. 1 shows the steel material stress-strain curve that was the result of monotonic and cyclic tests and the cyclic response calibration. Initially, the linear buckling analysis was done on the presence of a superficial load to the middle plate. The first buckling mode
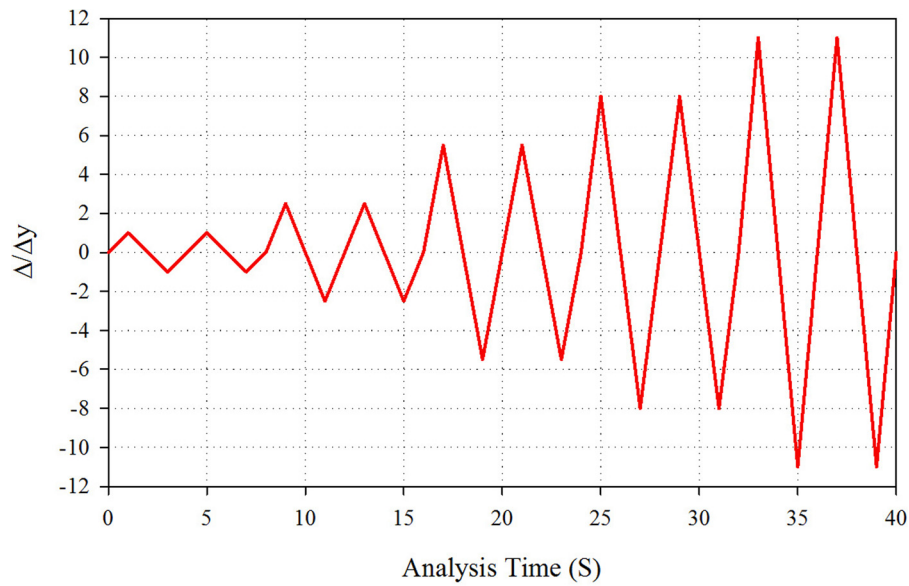

Fig. 2. Loading protocol of the BRB models according to AISC seismic provisions
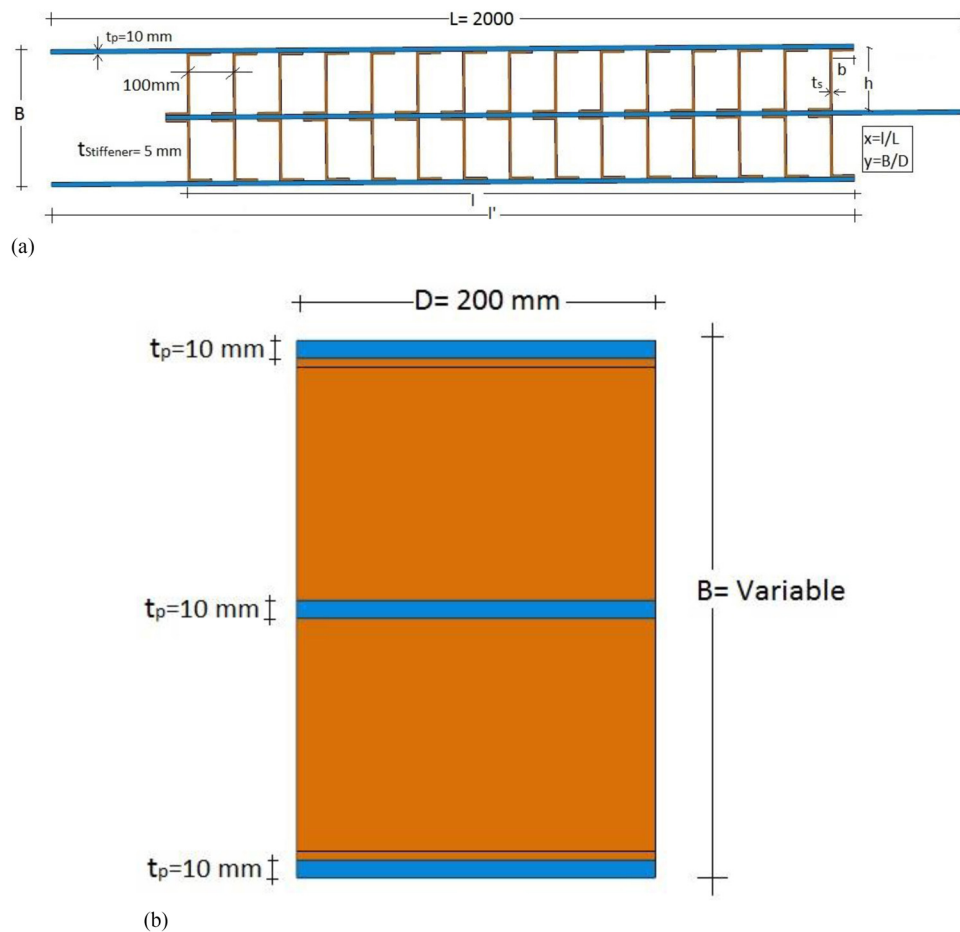

(a)

(b)

Fig. 3. Proposed BRB: (a) lateral view; (b) cross section with dimensions

was considered for models with geometrical imperfections. The boundary conditions in one end of the bracing were from hinge support, and the axial displacement toward the other ending of the same bracing entered into the end of the plate. Axial displacement applied to one side of the bracing was, as follows, per the cyclic pseudostatic loading protocol suggested by the AISC (2010a,b) regulations for BRBs: First, there were two cycles of $\pm\Delta_y$, followed by two cycles of $\pm0.5\Delta_{bm}$, two cycles of $\pm\Delta_{bm}$, two cycles of $\pm1.5\Delta_{bm}$, and ended with two final cycles of $\pm2\Delta_{bm}$, Δ_y steel core yield displacement, and Δ_{bm} bracing axial deformation in proportion to the floor drift (AISC 2010a). Considering the previously conducted study from Tremblay et al. (2006), the maximum strain throughout the bracing core for the common structural applications was between 0.01 and 0.02, and the maximum deformation in previous experimental studies was limited to be within the same range. In this paper, Δ_{bm} was considered 20 mm, which was in proportion to a core axial 1% strain, and Δ_y was equal to 3.24 mm. Therefore, the maximum bracing axial-deformation requirement within the traversed loading was approximately equal to 12 times Δ_y, representing a steel core strain of 2%. Fig. 2 shows the loading template. The proposed bracing meshed 3D section and the elevation are presented in Figs. 3 and 4.

Numerical Model Verification

This section explains the proposed numerical model that was validated by the results of the test specimen (Seker and Shen 2017). Brace sections were composed of two square-shaped sections, including the core of HSS 1.900×0.125 and the HSS $2\,1/2 \times 2\,1/2 \times 1/8$ type for the external sheath. The opening gap between

the two steel sections was 4.445 mm with a thickness of 3.2 mm. The total bracing length was equal to 1,270 mm. The yield stress of the core steel and the external sheath was 289 and 317 MPa, respectively. Fig. 5 shows the schematic of the bracing cross sections. The loading protocol was defined according to AISC regulations in the form of yield and designed displacements (Fig. 6). In this study, the design drift was considered to be equal to 2% of the floor height. The results of hysteresis behavior of the numerical model and experimental specimens (Seker and Shen 2017) are presented in Fig. 7. As seen, like the experimental model, the behavior of the numerical model was sustainable up to the eighth cycle, and from the ninth cycle, the strength of the specimen decreased at 1% of drift, because of the bending deformation generated in the bracing joint end plate. Meanwhile, when the drift reached 1.7% under a compressive state, a plastic area was generated at the external sheath ending.

Finite-Element Analysis Results

The hysteresis curves for all nine specimens are shown in Fig. 8. As expected, the maximum bracing axial stiffness was related to the specimens for which y of 0.5 was considered. On increasing the bracing section depth to the plate width ratio, the stiffness decreased for all specimens as shown in Fig. 9, for which the stiffness ratio was drawn by connecting the origin to the maximum load point of each cycle. According to Table 1, the maximum and minimum initial elastic stiffness was related to the $B_{0.75}G_{0.5}$ and $B_{0.25}G_{1.5}$ specimens with 250 and 12 kN/mm, respectively. By increasing the overlapping length, x, the initial elastic stiffness increased in a way that the maximum growth in the elastic stiffness was related to the
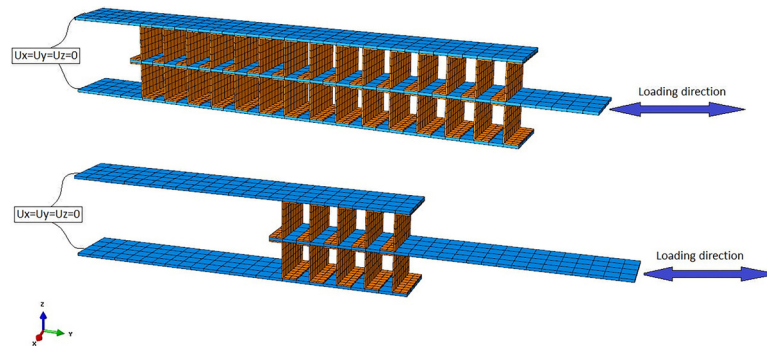

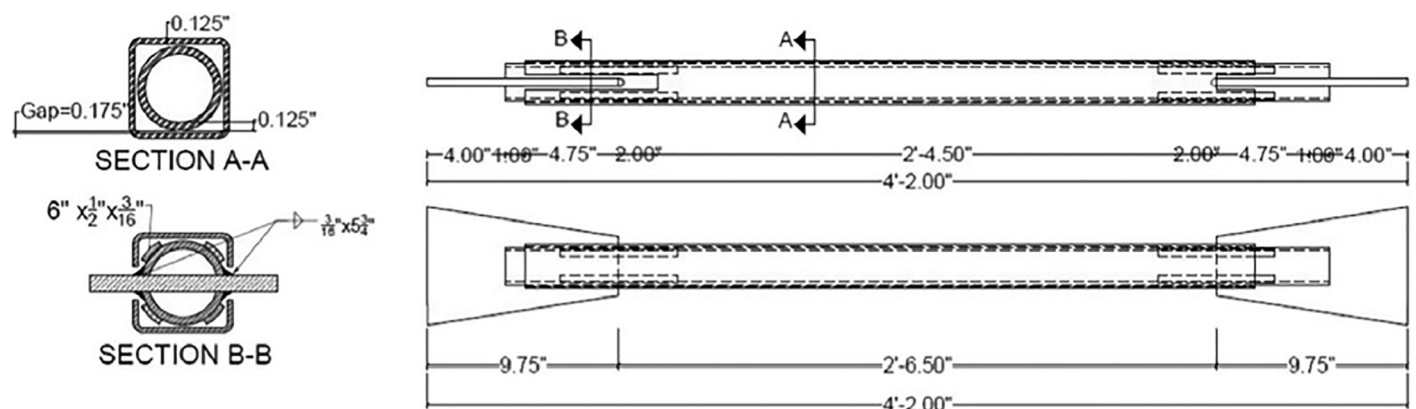**Fig. 4.** FE model and boundary conditions of the proposed BRBs

Fig. 5. Dimension and cross section of test specimens

© ASCE

04018016-4

Pract. Period. Struct. Des. Constr.

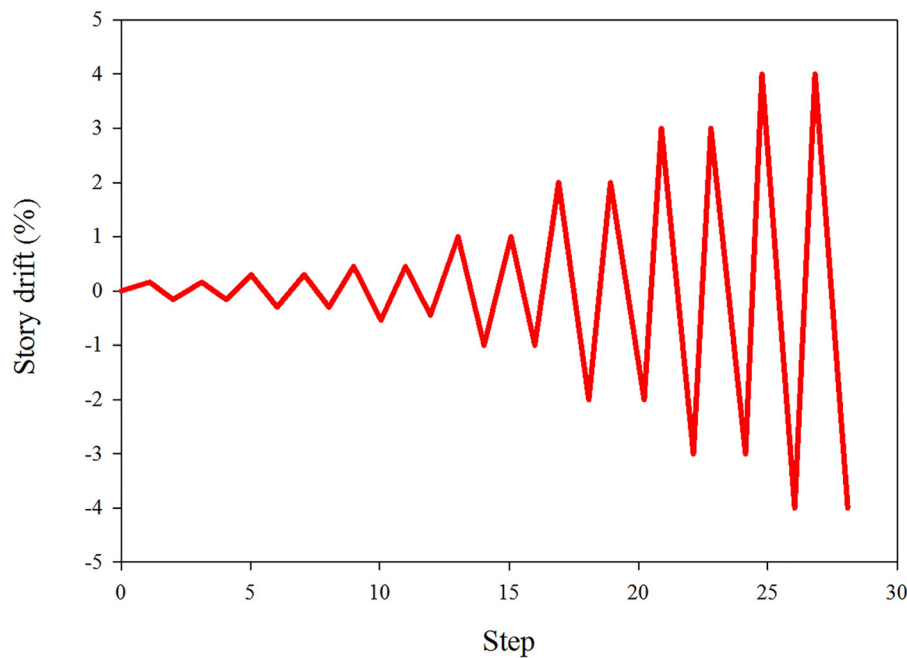Pract. Period. Struct. Des. Constr., 2018, 23(3): 04018016
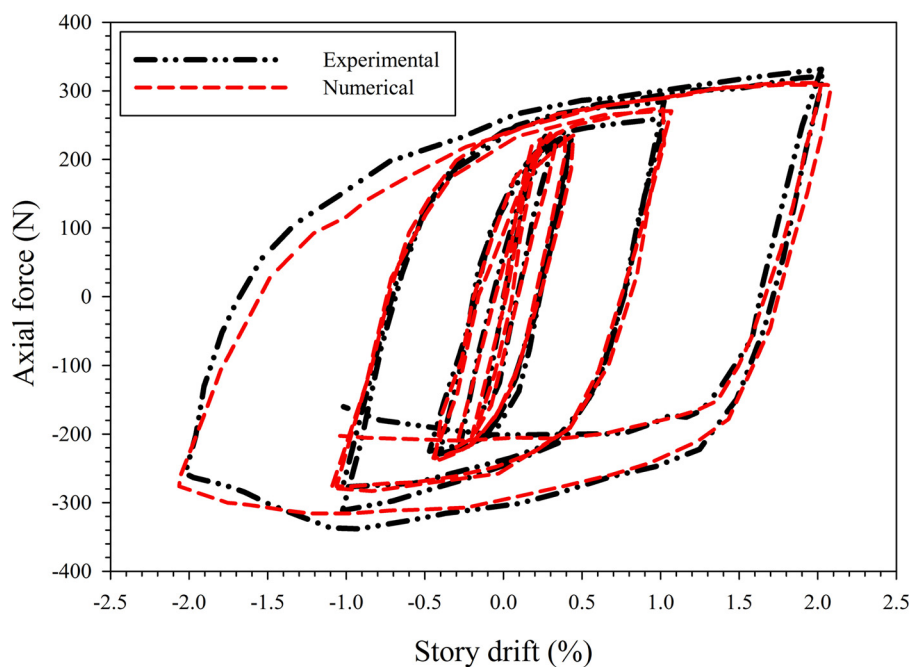
Fig. 6. Loading protocol

Fig. 7. Comparison of load-drift behaviors of the numerical model and the test specimens

$B_{0.75}G_{0.5}$ specimen. The bracing distance to the bracing length to width ratio significantly affected the bracing axial stiffness when the overlapping length was short. For instance, there was a 12-times stiffness increase for $B_{0.25}G_{1.5}$ specimen over the $B_{0.25}G_{0.5}$ specimen. Fig. 6 shows that by increasing the overlapping length of the bracing plates, the stiffness loss in different cycles decreased by changes in the bracing dimensional ratio (depth-to-width ratio). In Fig. 10, the final shapes of the suggested bracing specimens with stress and strain distributions are shown. It is true that a 200-mm axial displacement of the bracing was too much because it caused

significant plastic deformations. However, one should note that Z-shaped members were not solely able to bear the imposed deformation. If the entire ($x = 1$) middle plate and the two lateral plates were surrounded by Z-shaped profiles, then a 200-mm displacement would not be expected because the numerical analysis of the case in which the entire length of the middle plate was connected to a Z-shaped profile suggested that the maximum axial deformations determined by *Abaqus v6.14.2* software were 30, 80, and 120 mm for the Z-shaped profiles with a respective depth of 35, 85, and 135 mm. However, for cases in which a part of the total length of

© ASCE 04018016-5 Pract. Period. Struct. Des. Constr.

Pract. Period. Struct. Des. Constr., 2018, 23(3): 04018016
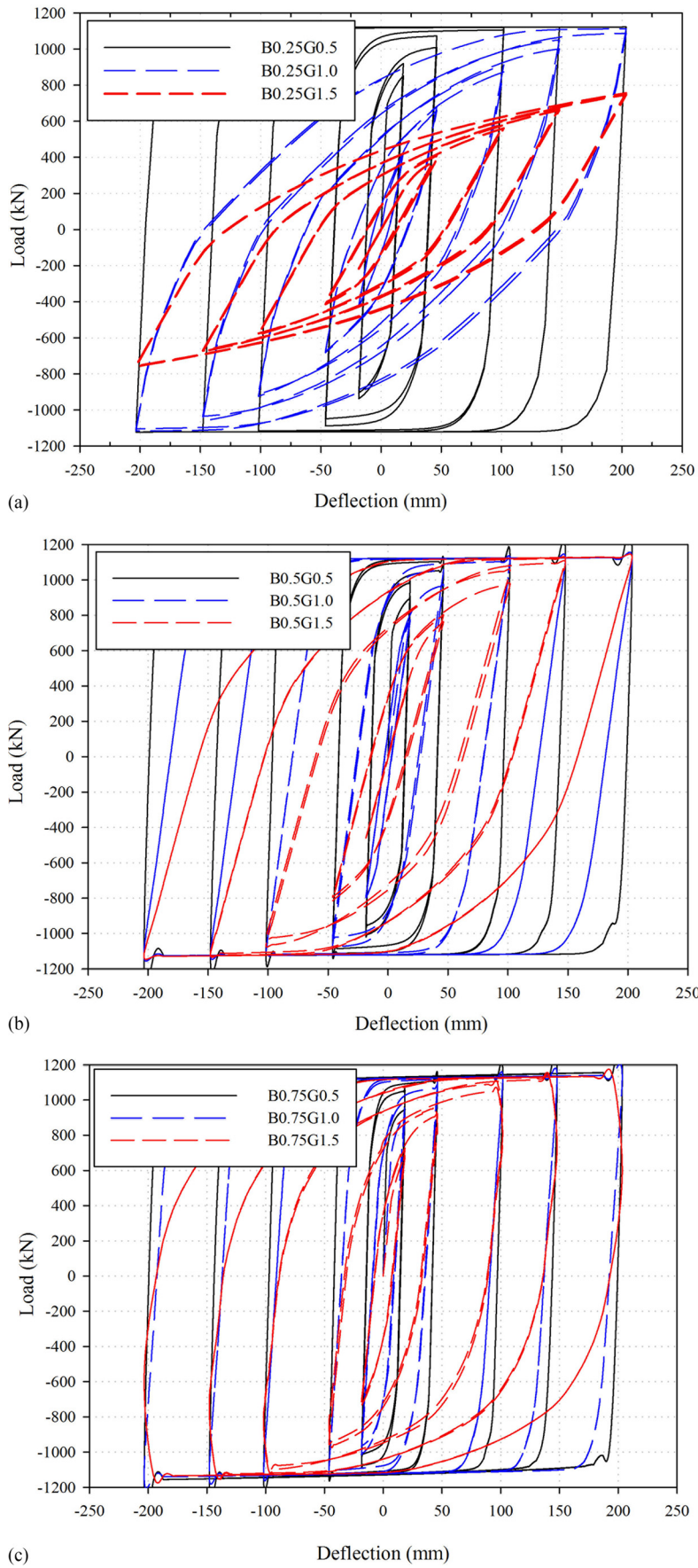
Fig. 8. Hysteretic and bilinear curves of the proposed BRBs by group: (a) $x = 0.25$; (b) $x = 0.50$; (c) $x = 0.75$

Fig. 9. Normalized lateral stiffness by BRB group: (a) $x = 0.25$; (b) $x = 0.50$; (c) $x = 0.75$

Fig. 10. Deformed shape and von Mises stress counter for two specimens of each type: (a) $B_{0.25}G_{0.5}$; (b) $B_{0.25}G_{1.0}$; (c) $B_{0.25}G_{1.5}$; (d) $B_{0.5}G_{0.5}$; (e) $B_{0.5}G_{1.0}$; (f) $B_{0.5}G_{1.5}$; (g) $B_{0.75}G_{0.5}$; (h) $B_{0.75}G_{1.0}$; (i) $B_{0.75}G_{1.5}$

the bracing was connected to a Z-shaped profile, the plastic defor-
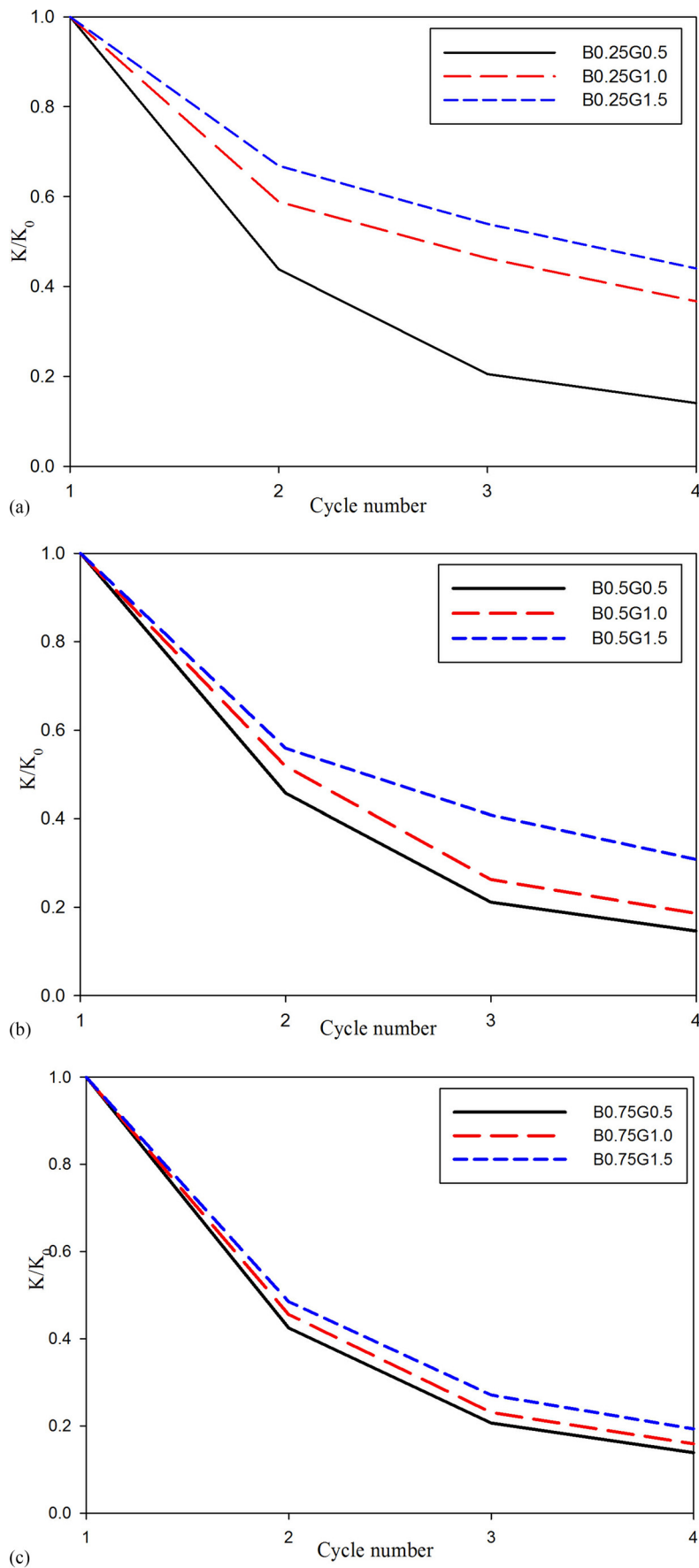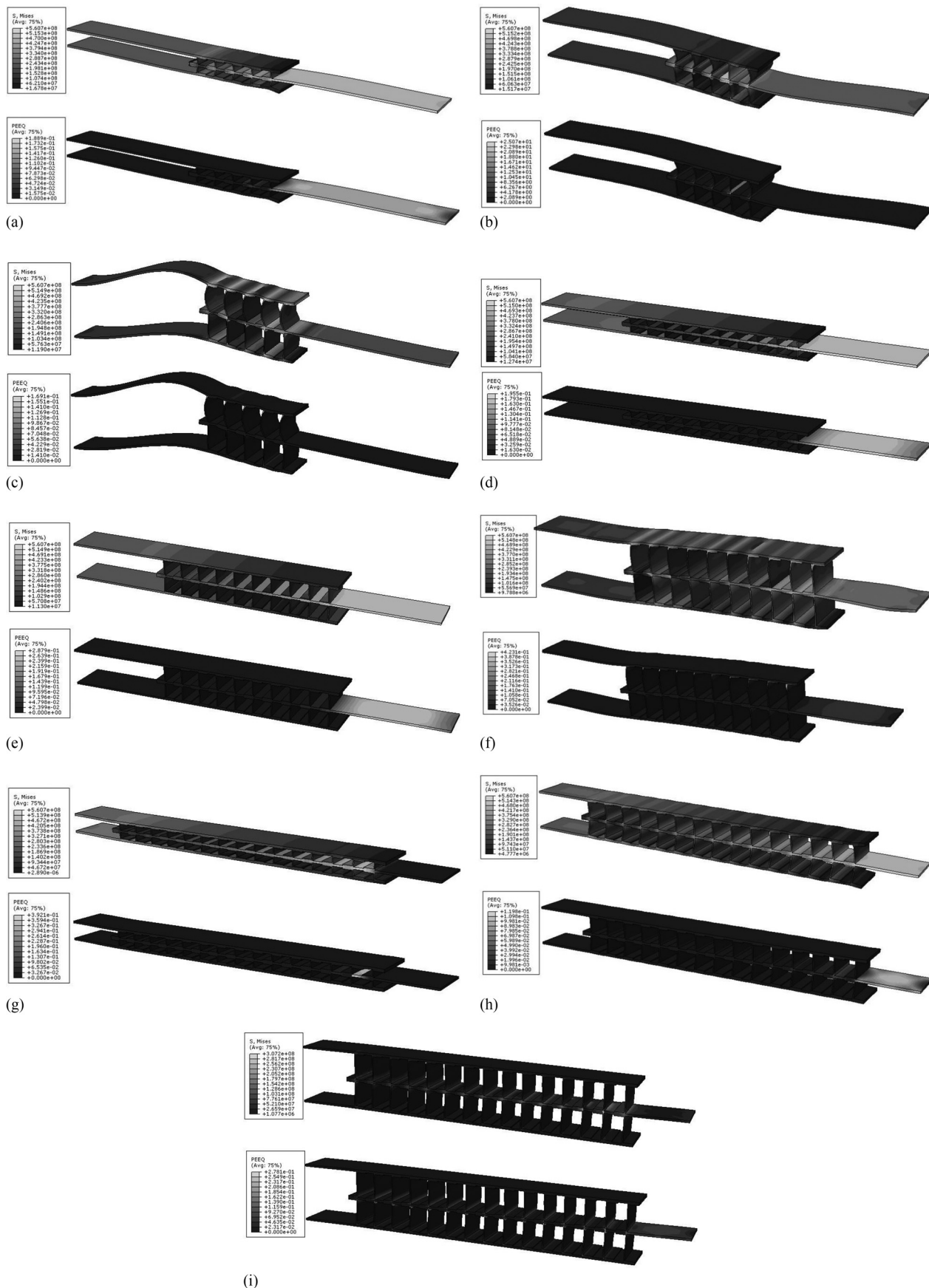mation of the profiles was accompanied by plastic deformations of
the plates (Fig. 10).

Fig. 11 shows the variations of the stress and strain in two
regions of the specimen $B_{0.75}G_{0.5}$. According to the curves in
Fig. 11, the plate adjacent to the loading location endured the

maximum plastic deformations. The top and bottom plates
remained elastic until the 20th cycle, while the Z-shaped pro-
files underwent severe plastic deformations. With the increasing
load for Element Number 2, it can be seen that plastic strain was
generated and the yielding regions extended throughout the
member.
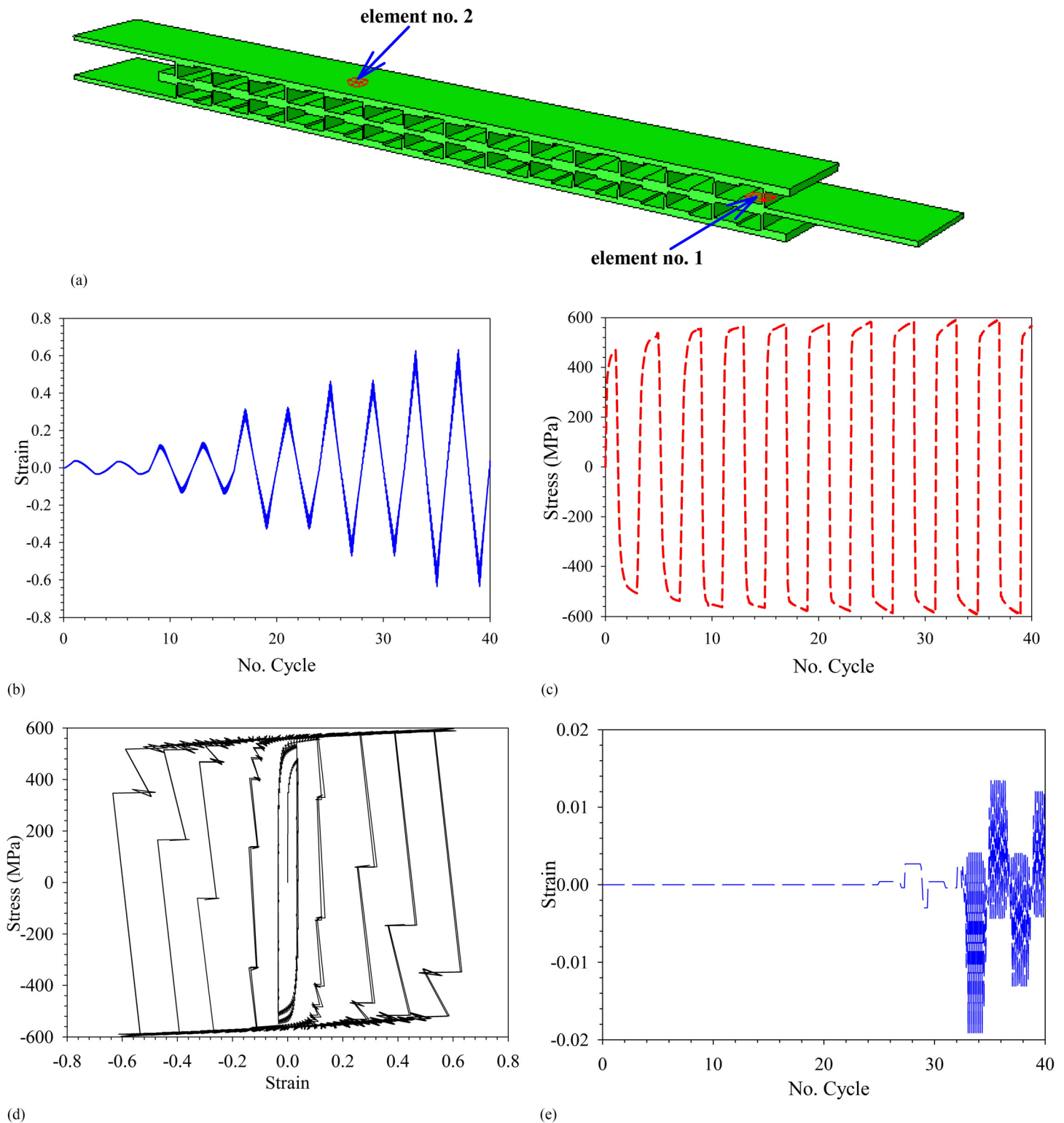
Fig. 11. Stress and strain distributions in specimen $B_{0.75}G_{0.5}$: (a) location of selected elements; (b) strain distributions of Element 1 through cycles;
(c) stress distributions of Element 1 through cycles; (d) stress-strain curve of Element 1; (e) strain distributions of Element 2 through cycles

© ASCE   04018016-9   Pract. Period. Struct. Des. Constr.

Pract. Period. Struct. Des. Constr., 2018, 23(3): 04018016

Nonlinear Static Analysis

In the nonlinear static stage, a pushover analysis was conducted to assess the performance of the proposed all-steel BRBs. Initially, a study was conducted to compare the steel structures braced with X-bracings. Then, such cross bracings were replaced by BRBs, and the structure was strengthened and the analyses were repeated.

In this study, three 5-, 10-, and 15-story structures were used to conduct the analyses. In Table 2, the particulars of the beam and column elements in the floors are presented. As shown, the height of each floor was considered to be 3 m. All three structures had a steel moment frame system, average formability with a special convergent bracing, and 15-m plan. Each structure included three spans, each 5 m in both directions, that are fully symmetric and regular in height and plan. Upon designing, the middle frame was selected and subjected to pushover analysis.

These frames were primarily subjected to structural design and seismic loading in the *SAP2000 v19.0.0* program according to AISC360-10 (AISC 2010b) and the Building and Housing Resource

Center (BHRC), Iranian Standard 2800 (BHRC 2015), respectively. The beam-to-column connections were modeled in a fully rigid manner, and the value for the live load and for the dead load for all the ceilings was 4.5 and 2 kN/m^2, respectively (except for the roof, where it was equal to 1.5 kN/m^2). The column sections were of a box type and the beams were of beam plate type. The CX-Y expression is used to refer to columns, where *C*, *X*, and *Y* refer to the column, column exterior dimensions in millimeters, and column thickness in millimeters, respectively. Fig. 12 shows the plan and frame with the bracing used before and after strengthening.

Fig. 13 shows the beam and bracing sections. Three frames of the 5, 10, and 15 floors were subjected to pushover nonlinear static analysis in the *SAP2000 v19.0.0*. To strengthen the frames, the all-steel BRBs with similar shapes to that of the $B_{0.75}G_{0.5}$ specimen were replaced by cross-bracing specimens. The statuses of the plastic hinges in the targeted displacement are shown in Fig. 14. The dimensionless push curve was used to model the BRBs according to the levels defined in FEMA 440 (FEMA 2005) and is shown in Fig. 15.

Table 2. Column, Beam, and Brace Dimensions

Number of stories	Story level	Column	Beam $[b_f \times h_w \times t_f \times t_w (\text{mm})]$	Brace $[b_b \times t_b (\text{mm})]$
5	1–3	C400-8	$110 \times 220 \times 10 \times 8$	80×8
	4–5	C350-8	$100 \times 200 \times 10 \times 8$	60×6
10	1–3	C500-15	$140 \times 300 \times 12 \times 8$	120×12
	4–6	C450-12	$140 \times 300 \times 12 \times 8$	100×10
	7–8	C350-12	$120 \times 240 \times 10 \times 8$	80×8
	9–10	C300-10	$100 \times 200 \times 10 \times 8$	80×8
15	1–3	C550-15	$170 \times 360 \times 15 \times 10$	160×14
	4–6	C500-12	$160 \times 340 \times 12 \times 10$	140×12
	7–9	C450-12	$150 \times 320 \times 12 \times 8$	120×12
	10–12	C350-12	$120 \times 260 \times 10 \times 8$	100×10
	13–15	C300-10	$100 \times 220 \times 10 \times 6$	80×8

Note: b_f = flange width; h_w = depth of web; t_f = thickness of flange; t_w = thickness of web; b_b = Width of brace; t_b = thickness of flange and web of brace.
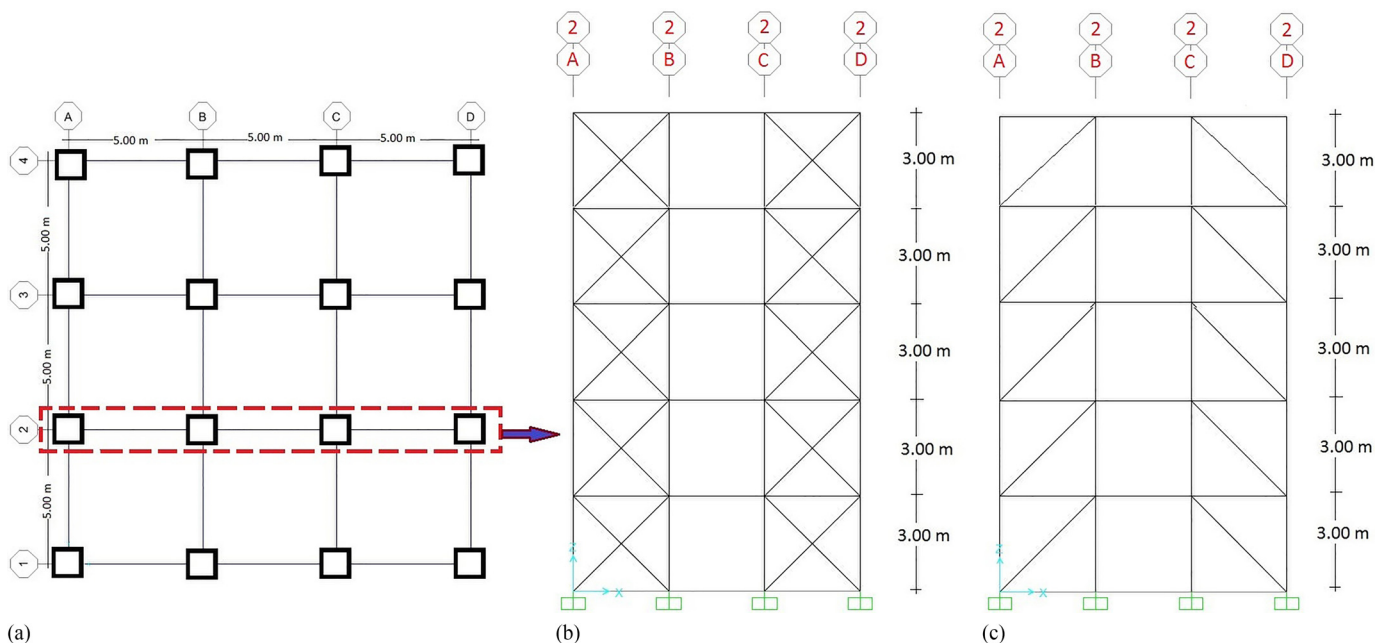

Fig. 12. Configuration of the 5-story braced frame before and after strengthening: (a) plan of the building; (b) before strengthening; (c) after retrofitting
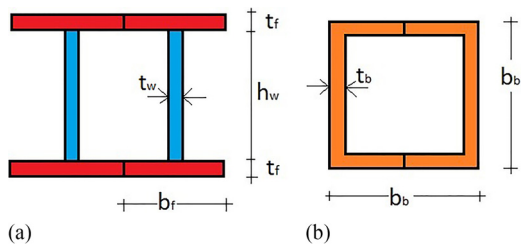
© ASCE   04018016-10   Pract. Period. Struct. Des. Constr.

Pract. Period. Struct. Des. Constr., 2018, 23(3): 04018016

Fig. 13. Configuration of the beam and X-brace sections: (a) beam; (b) brace

As shown in Fig. 14, the performance level of the structure equipped with a convergent cross bracing was promoted from the collapse threshold to the life-safety area by replacing the common cross bracings in the 5-floor frame by the proposed bracing. For instance, for 10- and 15-story buildings, the total frame performance level was promoted to life safety.

For the first floor columns, the axial forces before and after strengthening of each of the three frames are presented in Tables 3 and 4. The average axial force decrease was approximately 11%. In most cases, by decreasing the axial force value in the first floor columns, the average axial force value fell below that of the compressive and tension capacities of the columns.

Fig. 14. Five-story frame: (a) before retrofit; (b) after retrofit

Table 4. Axial Force Values of the First-Level Columns in X-Braced and Retrofitted Frames

Number of stories	Column label	X-braced frame (ton)	Retrofitted frame (ton)	Reduction in axial force (%)
5	A-2	312.6	276.2	34.1
	B-2	337.5	312.6	7.4
	C-2	346	308.1	11.0
	D-2	297.3	293	38.2
10	A-2	657.6	619.8	7.4
	B-2	710	702.4	1.1
	C-2	728	713.8	2.0
	D-2	625.4	605	12.7
15	A-2	794	762.3	4
	B-2	857.3	833.4	2.8
	C-2	878.8	817.4	7.0
	D-2	755	722.6	4.3
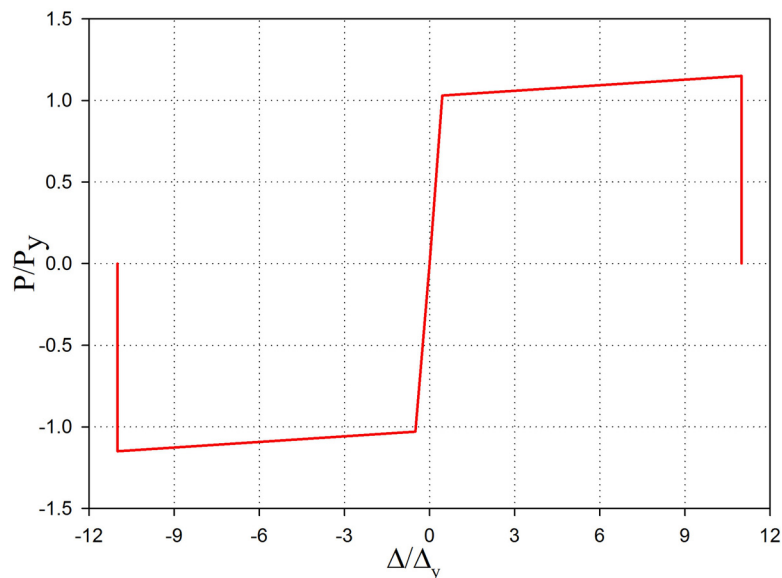
Fig. 15. Modeling parameters and acceptance criteria of BRB specimens

Table 3. Determination of Axial Forces Capacity

Number of stories	Section	Area (cm^2)	Slenderness factor	Length (cm)	Allowable stress (kg/cm^2)	Compressive capacity (kg)	Tensional capacity (kg)
5	C400-8	125	18.74	300	1,381.14	294,525	360,360
10	C500-15	291	15.14	300	1,394.55	689,884	844,093
15	C550-15	321	13.73	300	1,399.13	763,505	934,171

© ASCE

04018016-11

Pract. Period. Struct. Des. Constr.

Fig. 16. Pushover curve of frames

Fig. 17. General response of the structure during an earthquake
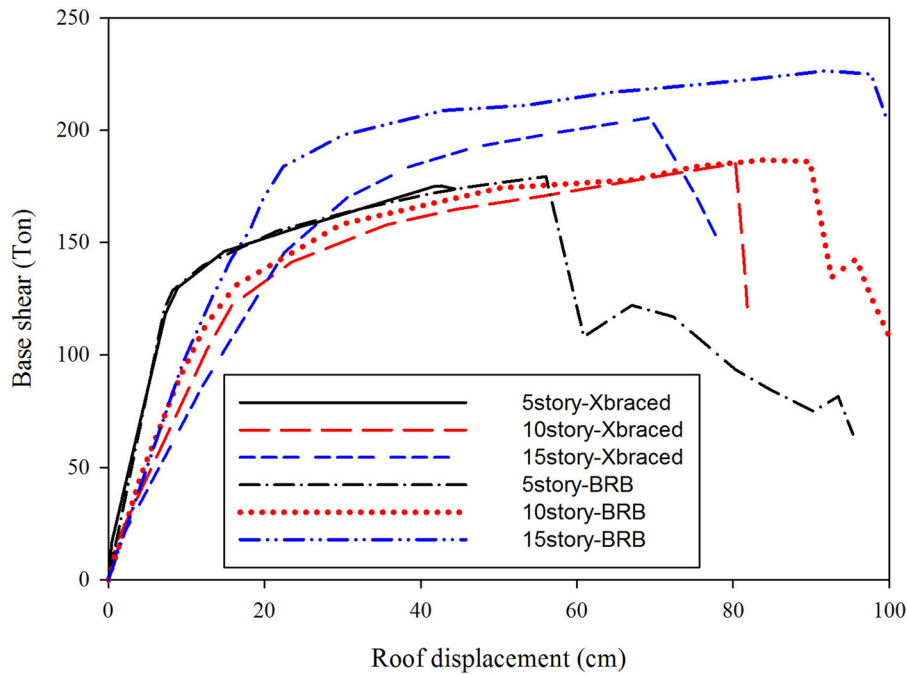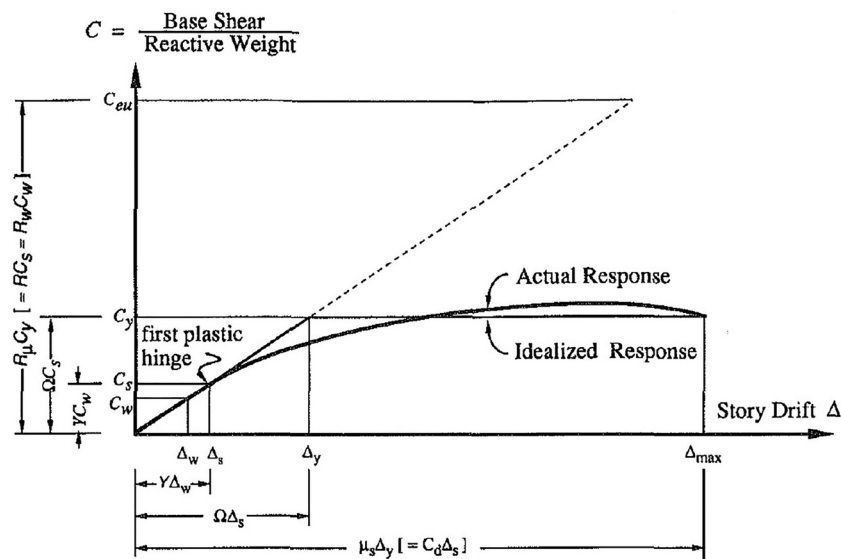
Meanwhile, the maximum decrease was related to the short 5-story building with different frames. In Fig. 16, the capacity curves of the frames resulting from the pushover analysis are shown for the frames with regular cross-convergent bracing and with BRBs.

As seen from the curves in Fig. 16, the presence of the suggested diagonal BRBs in the frames resulted in more ductile behavior than was found with regular cross-convergent bracing frames. The issue was the symmetric behavior of such types of bracing in tension and compression. The area under the curves represents the absorption capacity of the specimens, which was significantly high in specimens with the suggested BRBs. In other words, failure of the structures equipped with the suggested BRB was delayed because of the suitable formability.

Calculation of the Behavior Coefficient for Structures

In the seismic design instructions for building structures, the most challenging part is associated with force reduction and deflection amplification factors. The force decrease coefficient was expressed as the structure-behavior-modification coefficient, R, from the Building Seismic Safety Council (BSSC) in the National Earthquake Hazards Reduction Program (NEHRP) recommendations (BSSC 1997) or as the system performance coefficient, R_w, from the *Uniform Building Code* of the International Conference of Building Officials (1988) and the Structural Engineers Association of California (SEAOC) (SEAOC 1988). Fig. 17 shows the general structural response, and with it in mind, the ductility coefficient is calculated, in Eq. (1), as follows:

$$\mu_s = \frac{\Delta_{\max}}{\Delta_y} \tag{1}$$

Considering the ductility result, the structure has a certain capacity for energy absorption and depreciation. Because of the same energy absorption among structures, the elastic design force, C_y, may be decreased to the yield strength level using the R_μ coefficient as follows:

$$R_\mu = \frac{C_{eu}}{C_y} \tag{2}$$

The important point is that the yield strength level refers to structure failure level and not to the first yield level. The viscose damping ratio was considered as 5% for calculating such a decreased coefficient caused by ductility. For a system with one degree of freedom (DOF), the formula for determining the difference between the ductility and the decreased ductility coefficients comes from the formulas presented by Newmark and Hall (1982) and Riddell et al. (1989).

The remaining strength between the real structure yield level, C_y, and first effective yield level, C_s from the NEHRP regulations (BSSC 1997) are defined as the following overstrength coefficient:

$$\Omega = \frac{C_y}{C_s} = \frac{\Delta_y}{\Delta_s} \tag{3}$$

This overstrength of a structure resulted from the internal force distribution caused by the strength of the materials being greater than was considered in the design, including strain hardening, added section dimensions, combinations of different loadings, and effects of nonstructural elements, and the like.

The allowable stress coefficient was considered for the difference in materials by law. For designing an allowable stress method, the design force level. C_w, was decreased, as shown in Fig. 16, from the initial yield surface, C_s, with the Y coefficient as follows:.

$$C_w = \frac{C_s}{Y} \tag{4}$$

The Y value fell between 1.4 and 1.5. Eventually, the behavior coefficient in designing was calculated using the allowable stress method as follows in Eq. (5):

$$R = \frac{C_{eu}}{C_W} = \left(\frac{C_{eu}}{C_y}\right) \times \left(\frac{C_y}{C_S}\right) \times \left(\frac{C_s}{C_w}\right) = R_\mu \times \Omega \times Y \tag{5}$$

Meanwhile, the deflection amplification coefficient, C_d, which is the ratio between $\Delta_{\max}$ and Δ_s, may be calculated using Eq. (6) as

$$C_d = \mu_s \times \Omega \tag{6}$$

In Table 5, the overstrength, ductility, and behavior coefficients and the deflection amplification factors for the frames, before and after strengthening, are presented. Considering the results, the structural response modification coefficient with the proposed BRB was bigger than the frame system with regular cross convergent bracing because the BRBs had a higher ductility coefficient. Meanwhile, from the results, it was inferred that upon increasing the structure height, the structure behavior coefficient decreased.

Nonlinear Time-History Analysis

Finally, the nonlinear time-history analysis was carried out for two states of frames before and after strengthening, and the results took the form of the distribution floor drift ratio for each accelerogram. The particulars of the two accelerograms of the near field and the two accelerograms of the far field are listed in Table 6 with respect to FEMA P695 suggestions (FEMA 2009). In Fig. 18, a comparison is shown between the floor drift ratios in all the models without and with strengthening in quakes of both near and far fields. Considering the results, the floor drift ratio for the strengthened frames was a little less than it was for the frames with regular cross-convergent bracing. The symmetric behavior of the cross-convergent bracings may be an acceptable

Table 5. Response Modification Factors of All-Steel BRBs and X-Braced Frames

Number of stories	Type of frame	Ω	R_μ	R	C_d
5	Proposed BRB	1.73	5.78	11.64	6.78
10	Proposed BRB	1.69	5.77	10.75	6.15
15	Proposed BRB	1.46	3.15	8.13	5.13
5	X-bracing	1.48	4.03	8.92	3.33
10	X-bracing	1.65	3.76	7.33	3.67
15	X-bracing	1.32	2.51	5.29	3.54

Table 6. Earthquake Data for the Parametric Analysis (Data from PEER 2015)

Earthquake motion parameters	Northridge earthquake (USA)	Kobe (Japan)	El Centro (USA)	Hachinohe (Japan)
Date of occurrence (year)	1994	1995	1940	1968
Magnitude of earthquake (M_w)	6.7	6.8	6.9	7.5
Maximum horizontal acceleration (g)	0.843	0.834	0.349	0.231
Predominant period [$T_p(s)$]	0.36	0.36	0.56	0.22
Significant duration [$D_{5-95}(s)$]	5.32	8.4	24.58	27.79
Time of MHA [$t_p(s)$]	4.2	8.52	4.1	4.18
PGV/PGA (s)	0.157	0.112	0.102	0.146
Arias intensity (m/s)	5.004	8.389	1.758	0.899
SIR (m/s/s)	1.903	1.407	0.117	0.037
Energy flux ($J \cdot m^{-2} \cdot sec^{-1}$)	8,560.187	7,649.179	2,144.177	2,409.691
Type	Near field	Near field	Far field	Far field
Hypocentral distance (km)	9.2	7.4	15.69	14.1

Note: $SIR = I_{a(5-75)}/D_{(5-75)}$; PGV/PGA = peak ground velocity to peak ground acceleration.

© ASCE   04018016-13   Pract. Period. Struct. Des. Constr.

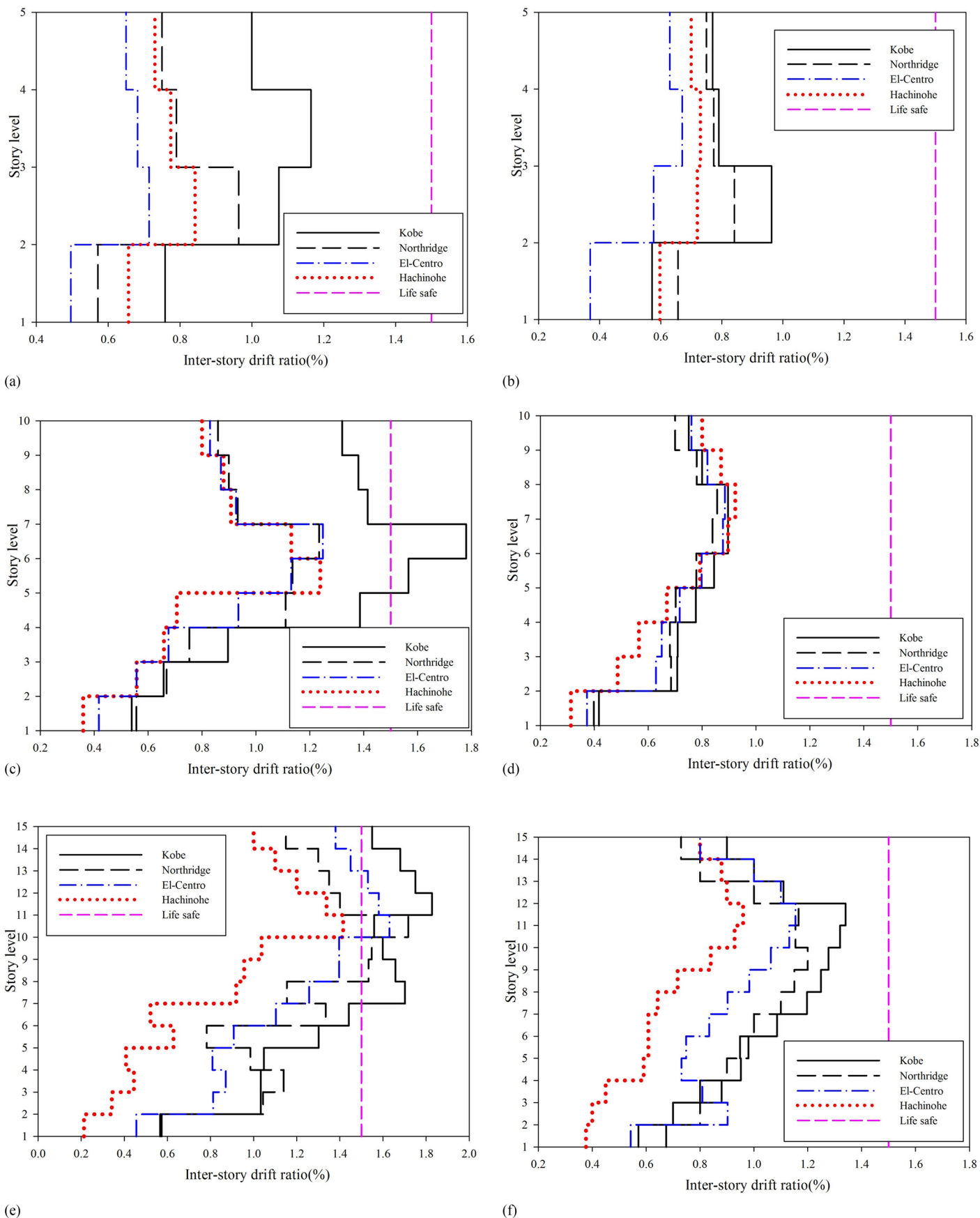Pract. Period. Struct. Des. Constr., 2018, 23(3): 04018016

Fig. 18. Interstory drift ratio of structures: (a) 5-story X-braced drift ratio; (b) 5-story BRB-braced drift ratio; (c) 10-story X-braced drift ratio; (d) 10-story BRB-braced drift ratio; (e) 15-story X-braced drift ratio; (f) 15-story BRB-braced drift ratio

explanation for this difference; that is, the regular bracings were subjected to strength loss and yield after a couple of cycles because of buckling problems.

Performance levels were used to describe the state of the structures after being subjected to a certain hazard level, and those based on FEMA 273 (FEMA 1997) were classified as fully operational, operational, life safe, near collapse, and collapse. Overall lateral deflection, ductility demand, and interstory drifts were the most commonly used damage parameters. Each of the five qualitative levels was related to a corresponding quantitative maximum interstory drift (as a damage parameter) as follows: $< 0.2, < 0.5, < 1.5, < 2.5,$ and $> 2.5\%$, respectively.

The floor drift ratio charts show that the regular bracings in a 5-story low building managed to keep the structure within the life-safety region under both the near-field and far-field types of time histories. However, when the number of floors was increased from 5 to 10, it was seen that the structure with the regular cross-convergent bracings shown in the accelerogram for the near field of Kobe failed to remain in the life-safety region. By replacing the X-bracings with the suggested BRBs, the structure performance level was kept in the life-safety region. For those of 15-story frames, the structure was at collapse in all the near-field and far-field accelerograms, while the structure performance level to the life-safety level was changed through strengthening. Considering these results, it can be inferred that the maximum floor drift ratio was generated with the near-field accelerogram, and that such an effect was seen more often in tall structures.

Concluding Remarks

The new BRBs introduced in this study were composed of three steel plates with fittings among the plates from Z-shaped profiles. The role of the parallel plates was to provide the required stiffness and strength to transfer the load and meet the desirable performance of plates that have the duty of energy absorption in the system. Absorbing energy in the system was done through formation of plastic hinges in plates placed in the system with respect to the weak axis. The height and thickness of the plates placed in the suggested bracing system were varied, and the strength, stiffness, and ductility of the system were changed by changing the number, thickness, and height of the plates used. The advantage of this system in comparison to other bracing systems included the logical directing of the compressive forces inside the members and converting the same forces into bending and sharing forces, through which, in addition to preventing premature failure of members, the energy absorbability in the system significantly improved. In addition, the stiffness and strength of the two deterministic factors in the system resisted the lateral loads. In this paper, first by changing the length parameters of the overlapping plates and the dimensional ratio of the bracing width to depth, several analyses were made in the *Abaqus v6.14.2* FE program to determine the nonlinear modeling parameters. Then, the performances of the 5-, 10-, and 15-story frames equipped with the suggested system were studied and evaluated precisely using the *SAP2000 v19.0.0* program through push-over and nonlinear time-history analyses. An abbreviated summary of the analyses findings is presented as follows:

- By increasing the bracing depth-to-width plate ratio, the stiffness in the specimen decreased. By increasing the overlapping length, the initial elastic stiffness increased such that the maximum growth in elastic stiffness was related to the $B_{0.75}G_{0.5}$ specimen for which the ratio was approximately 5.5 times greater than it was for the $B_{0.25}G_{0.5}$ specimen. The effect of the dimensional ratio of the distance between two plates to the

width was quite significant in increasing the bracing axial stiffness when the overlapping length was small.

- Using the $B_{0.75}G_{0.5}$ full-steel BRBs in strengthening the 5-, 10-, and 15-story frames resulted in keeping the structure performance level in the life-safety region as shown in the pushover analyses. In contrast, the performance level for 10- and 15-story frames with X-bracings entered into the failure region.
- The axial forces of the first floor columns strengthened in a 5-story frame had a 22.7% decrease compared to those for the frame without strengthening. The maximum value of this decrease was 5.8 and 4.5% for the 10- and 15-story frames, respectively. The stiffness in the strengthened steel structures, especially in the connection locations, seemed to provide a good excuse for using all-steel BRBs, which also decrease the axial forces in the column and the size.
- The behavior and ductility factors for all-steel BRBs were approximately 44 and 41% greater than they were for the frames equipped with regular cross bracings. Evidently, the taller frames had less ductility and a smaller behavior coefficient.
- The average of the maximum floor drift ratio for the 5-, 10-, and 15-story was decreased by 13, 31, and 30%, respectively, in the far-field accelerograms. The taller frame (15-story) managed to remain in life-safety region, and by using the all-steel BRBs, this problem was addressed.
- The decrease in the floor drift ratio in strengthened 5-, 10- and 15-story frames, with respect to the same frames with regular cross-convergent bracings, was 11.5, 41, and 30% for near-field quakes. Unlike the far field, in the 10-story frame of the Kobe accelerogram, the cross-bracing frame performance showed an exit from the life safety-region, and for the 15-story frame, the performance entered into the failure stage in both types of accelerograms. Using the proposed diagonal BRBs increased the performance levels such that they were changed to life-safety areas.

References

Abaqus v6.14.2 [Computer software]. SIMULIA, Providence, RI.

AISC. (2010a). "Seismic provisions of structural steel building." *ANSI/AISC 341-10*, Chicago.

AISC. (2010b). "Specification for structural steel buildings." *ANSI/AISC 360-10*, Chicago.

BHRC (Building and Housing Resource Center). (2015). "Iranian Building Codes and Standards, Iranian Code of Practice for Seismic Resistant Design of Buildings 4th Ed." *Iranian National Standard 2800*, Tehran, Iran.

Black, C., Makris, N., and Aiken, I. (2002). "Component testing, stability analysis and characterization of buckling-restrained braces." *PEER Rep. 2002/08*, Pacific Earthquake Engineering Research Center, Univ. of California, Berkeley, CA.

BSSC (Building Seismic Safety Council). (1997). "The NEHRP (National Earthquake Hazards Reduction Program) recommended provisions for the development of seismic regulations for new buildings. "Building Seismic Safety Council, Washington, DC.

Fahnestock, L. A., Ricles, J. M., and Sause, R. (2007). "Experimental evaluation of a large-scale buckling-restrained braced frame." *J. Struct. Eng.*, 10.1061/(ASCE)0733-9445(2007)133:9(1205), 1205–1214.

FEMA. (1997). "NEHRP guidelines for the seismic rehabilitation of buildings." *FEMA 273*, Washington, DC.

FEMA. (2005). "Improvement of Nonlinear Static Seismic Analysis Procedures." *FEMA 440*, Washington, DC.

FEMA. (2009). "Quantification of Building Seismic Performance Factors." *FEMA P695*, Washington, DC.

Hosseinzadeh, Sh., and Mohebi, B. (2016). "Seismic evaluation of all-steel buckling restrained braces using finite element analysis." *J. Constr. Steel Res.*, 119(Dec), 76–84.

© ASCE   04018016-15   Pract. Period. Struct. Des. Constr.

Pract. Period. Struct. Des. Constr., 2018, 23(3): 04018016

Hoveidae, N., and Rafezy, B. (2012). "Overall buckling behavior of all-steel buckling restrained braces." *J. Constr. Steel Res.*, 79(Dec), 151–158.

International Conference of Building Officials. (1988). "Uniform building code." Whittier, CA.

Kimura, K., Yoshizaki, K., and Takeda, T. (1976). "Tests on braces encased by mortar infilled steel tubes." *Summaries of technical papers of annual meeting, AIJ*, Architectural Institute of Japan, Tokyo, 1041–1042.

Korzekwa, A., and Tremblay, R. (2009). "Numerical simulation of the cyclic inelastic behavior of buckling restrained braces." *Proc., Int. Specialty Conf., Behaviour of Steel Structures in Seismic Areas: STESSA 2009*, F. Mazzolani, J M. Ricles, and R. Sause, eds., CRC, Boca Raton, FL.

Merritt, S., Uang, C.-M., and Benzoni, G. (2003). "Subassemblage testing of corebrace buckling-restrained braces." *Rep. TR-2003/01*, Univ. of California, San Diego, San Diego, CA.

Mochizuki, S., Murata, Y., Andou, N., and Takahashi, S. (1979). "Experimental study on buckling of unbonded braces under axial forces: Parts 1 and 2." *Summaries of technical papers of annual meeting, AIJ*, Architectural Institute of Japan, Tokyo, 1623–1626.

Newmark, N. M., and Hall, W. J. (1982). *Earthquake spectra and design*, Earthquake Engineering Research Institute, Berkeley, CA.

PEER (Pacific Earthquake Engineering Research Center). (2015). PEER ground motion database, Univ. of California, Berkeley, CA.

Riddell, R., Hidalgo, P., and Cruz, E. (1989). "Response modification factors for earthquake resistant design of short period buildings." *Earthquake Spectra*, 5(3), 571–590.

SAP2000 19.0.0 [Computer software]. Computers and Structures, Inc., Walnut Creek, CA.

SEAOC (Structural Engineers Association of California). (1988). "Recommended lateral force requirements and tentative commentary. Seismological committee." San Francisco, CA.

Seker, O., and Shen, J. (2017). "Developing an all-steel buckling controlled brace." *J. Constr. Steel Res.*, 131(Apr), 94–109.

Tremblay, R., Bolduc, P., Neville, R., and Devall, R. (2006). "Seismic testing and performance of buckling-restrained bracing systems." *Can. J. Civ. Eng.*, 33(2), 183–198.

Tsai, K.-C., and Hsiao, P.-C. (2008). "Pseudo-dynamic test of a full-scale CFT/BRB frame—Part II: Seismic performance of buckling-restrained braces and connections." *Earthquake Eng. Struct. Dyn.*, 37(7), 1099–1115.

Tsai, K.-C., Lai, J.-W., Hwang, Y.-C., Lin, S.-L., and Weng, C.-H. (2004). "Research and application of double-core buckling restrained braces in Taiwan." *Proc., 13th World Conf., Earthquake Engineering*, Canadian Association for Earthquake Engineering, International Association for Earthquake Engineering, Vancouver, Canada.

Tsai, C. S., Su, H. C., and Chiang, T. C. (2012). "Huge scale tests of all-steel multi-curve buckling restrained braces." *Proc., 15th World Conf., Earthquake Engineering (15WCEE)*, Sociedade Portuguesa de Engenharia Sismica, Lisbon, Portugal.

Wada, A., Saeki, E., Takeuchi, T., and Watanabe, A. (1989). "Development of unbonded brace." *Column Technical Publication No. 115 1989.12*, Nippon Steel, Japan.

Wakabayashi, M., Nakamura, T., Katagihara, A., Yogoyama, H., and Morisono, T. (1973). "Experimental study on the elastoplastic behavior of braces enclosed by precast concrete panels under horizontal cyclic loading—Parts 1 & 2." *Summaries of technical papers of annual meeting*, Kinki Branch of Architectural Institute of Japan, Japan, Vol. 6, 121–128.

Zhao, J., Wu, B., and Ou, J. (2011). "A novel type of angle steel buckling-restrained brace: Cyclic behavior and failure mechanism." *Earthquake Eng. Struct. Dyn.*, 40(10), 1083–1102.

Zhu, B.-L., Guo, Y.-L., Zhou, P., Bradford, M. A., and Pi, Y.-L. (2017). "Numerical and experimental studies of corrugated-web-connected buckling-restrained braces." *Eng. Struct.*, 134, 107–124.

© ASCE   04018016-16   Pract. Period. Struct. Des. Constr.

Pract. Period. Struct. Des. Constr., 2018, 23(3): 04018016